Powder Technology 283 (2015) 227–233

Contents lists available at ScienceDirect

Powder Technology

journal homepage: www.elsevier.com/locate/powtec

Experimental and analytical study of the motion of a sphere falling along an inclined plane in still water

Román Martino [a,*], Agnes Paterson [b], Marcelo F. Piva [a]

[a] Grupo de Medios Porosos, Facultad de Ingeniera, Universidad de Buenos Aires, Paseo Colón 850 (1063), Buenos Aires Argentina
[b] Departamento de Hidráulica, Facultad de Ingeniera, Universidad de Buenos Aires, Las Heras 2214(1127), Buenos Aires Argentina

ARTICLE INFO

Article history:
Received 22 December 2014
Received in revised form 6 May 2015
Accepted 17 May 2015
Available online 24 May 2015

Keywords:
Submerged inclined plane
Rolling sphere
Accelerated motion
Terminal velocity

ABSTRACT

In this work, the transient regime of motion of a sphere, that falls along an inclined smooth plane, submerged in still water, is studied experimentally and analytically. Several experiments were performed, with spheres of different diameters and densities, and two slope angles. The measurements show that the motion of the sphere presents two well defined stages: a transitional regime, where the sphere rapidly accelerates from rest, and an asymptotic regime, where the sphere moves with constant velocity. Closed expressions, for the position and velocity of the sphere as functions of time, are obtained by direct integration of the motion equations. This theoretical analysis is based on the empirical correlation for the drag coefficient as a function of the Reynolds number of the sphere, that was proposed by Chhabra and Ferreira [2] for the experimental data set of Jan and Chen [1]. The analytical solution shows good agreement with experimental results, for a wide range of experimental conditions.

1. Introduction

The description of the motion of a spherical particle, that moves under gravity along an inclined plane submerged in a quiescent fluid, is a common topic in the study of the problems related with sediment deposition and solid classification (in urban drainage, sewers and water treatment plants, among other examples).

In many cases, the main parameter to predict is the so-called terminal velocity of the center of mass of the spheres, U_t (the velocity that is reached when gravitational and resistive forces are in equilibrium), given the slope of the plane, θ, and the properties of both, the fluid (density, ρ, and viscosity, μ) and the spheres (diameter, d, and density, ρ_p).

The work of Jan and Chen [1] presents measurements of U_t, for a sphere rolling down along a smooth plane, submerged in several incompressible Newtonian fluids, for slopes in the range $2° \le \theta \le 10°$. The authors present a correlation between the drag coefficient, C_D (that quantifies the total hydrodynamic resistance over the sphere), and the Reynolds number of the sphere, $Re = U_t d / \nu$, where $\nu = \mu / \rho$ is the kinematic viscosity. One of the main results of this work is the dimensionless graphs that allow determining of U_t and L_t, which is the distance traveled by the sphere until U_t is attained, as a function of θ, ρ, μ, d, and ρ_p.

Chhabra and Ferreira [2] present a set of differential equations, valid for the motion of a single rigid sphere, rolling down a smooth inclined plane submerged in a Newtonian fluid, assuming a non-slip condition between sphere and plane. After integration of these equations with respect to U_t, the authors derive equations to calculate the dimensionless numbers for acceleration, distance and time, as functions of the terminal Reynolds number. The authors used the following correlation of C_D against Re, that fits the results of Jan and Chen [1] previously cited:

$$C_D = A + \frac{B}{Re} \tag{1}$$

with $A = 0.861$ and $B = 321.906$, the above expression provides the best fit in the range $0.1 \le Re \le 10^5$, with an average relative deviation of 11%. The authors show that if $Re << B/A$ the viscous drag dominates, while if $Re >> B/A$ an inertial regime of motion takes place, with almost constant values of C_D.

Eq. (1) was also used by Jalaal and Ganji [3] in an analytical study of the unsteady motion of a sphere rolling down an inclined plane submerged in a Newtonian fluid. The authors apply the homotopy perturbation method (HPM) to construct a solution for the time evolution of the velocity of the center of mass of the sphere, $U(t)$. A comparison with the numerical solution of the differential equations shows the effectiveness of the proposed method, when applied to that kind of problems.

In the same way, Ebrahimi et. al. [4] also use Eq. (1) to construct a solution for the evolution with time of the velocity and the position of the center of mass of a sphere, $U(t)$ and $X(t)$, respectively, when the sphere is rolling down along an inclined smooth plane submerged in a Newtonian fluid. Unlike the previous cited work, the authors used the differential transformation method (DTM), based upon a Taylor series

* Corresponding author.
E-mail address: rmartino@fi.uba.ar (R. Martino).

http://dx.doi.org/10.1016/j.powtec.2015.05.022
0032-5910/

expansion. The comparison with the numerical solution, obtained with a Runge–Kutta scheme, demonstrates that the DTM method can achieve suitable predictive results.

Verekar and Arakari [5] presented experimental results for the motion of acrylic spheres, $\rho_p = 1.18\ g/cm^3$, with two diameters: 2.54 cm and 5.08 cm, rolling down along an inclined plane submerged in a tank 15 cm in width. They numerically solved the differential equation of motion to obtain $U(t)$ and $X(t)$ for a sphere, that is released from rest, and, as in the previous cases, they also used Eq. (1) in modeling the drag force over the sphere. When the authors compared this numerical solution with measurements, they observed that the model follows the main trends of the experimental results if one uses an added-mass coefficient lower than those proposed by Jan and Chen [1].

It can be concluded that the study of the accelerated initial phase of the motion of a sphere, falling from rest along a submerged inclined plane, has received much less attention, in comparison with the amount of studies devoted to the asymptotic regime of motion, with constant terminal velocity.

In this work, we study experimentally the motion of solid spheres falling, from rest, along a smooth inclined plane, submerged in quiescent water. With the aim to investigate the transient part of the motion of the sphere, and the way the stationary regime of motion is reached with time, a video recording technique was used to obtain, with high temporal resolution, the trajectory of the center of mass of the sphere. As a result, it was possible to measure the accelerated phase of the motion with high accuracy, along the almost straight paths followed by the spheres. In addition, small lateral departures from these straight trajectories were also detected. Several tests were performed using two slope angles. For each one, the objective was to quantify the influence of diameter and density on the transient motion of the sphere, from rest until reaching its terminal velocity. Solving the dynamic equations of motion, a set of closed analytical expressions of $X(t)$ and $U(t)$ was obtained, under the assumptions that the sphere behaves as a rigid body, rolling down, without sliding, along an inclined smooth plane, submerged in a quiescent fluid, that is assumed Newtonian and incompressible. Based in the results of the previous works cited above, Eq. (1) is used to model the drag force on the sphere. The predictions from these analytical equations are compared with our own measurements, as well as with the results provided by the other authors previously cited.

This paper is organized as follows: Section 2 is devoted to the analytical solution of the equation of motion, in Section 3, the experimental results are presented and discussed, and, finally, conclusions are offered in Section 4.

2. Problem definition and derivation of the analytical solution

Fig. 1 shows the free body diagram for a single sphere of diameter $d = 2r$ and mass $m = \rho_p 4/3\pi r^3$, r and ρ_p are the radius and the density of the sphere, respectively. The sphere is rolling down over a smooth inclined plane, submerged in a quiescent fluid with dynamic viscosity μ and density ρ. The slope of the plane is given by the angle θ.

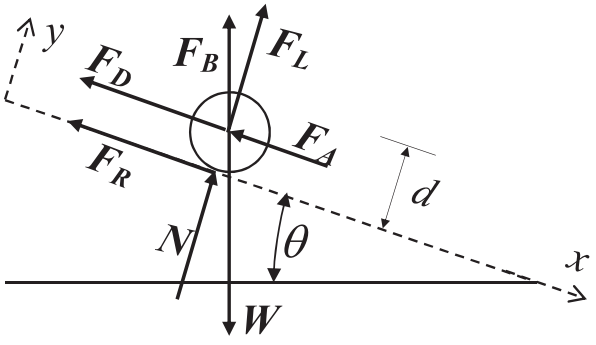

Fig. 1. Free body diagram for a single sphere rolling down along an inclined submerged plane.

The forces acting over the sphere are: drag: F_D, lift; F_L, weight: $W = mg = \rho_p 4/3\pi r^3 g$, buoyancy: $F_B = \rho 4/3\pi r^3 g$, normal reaction from the plane: N, rolling resistance: F_R, and an inertia force of added mass: F_A, that is included because acceleration of the sphere implies acceleration of the surrounding fluid. As in previous works, since we are working with a dense sphere submerged in a light liquid, the term associated with Basset forces is neglected in first approximation [2].

Assuming that the sphere behaves as a rigid body, the summation of forces along the inclined plane (x-axis) leads to the following equation:

$$-C_D\frac{1}{2}\rho U^2\pi r^2 + \Delta\rho\frac{4}{3}\pi r^3 gSin(\theta) - C_A\rho\frac{4}{3}\pi r^3\frac{dU}{dt} - F_R = \rho_p\frac{4}{3}\pi r^3\frac{dU}{dt} \quad (2)$$

where the first term in the left hand side is the drag force, and the second is the submerged weight (W–F_B) projected along the plane, where $\Delta\rho = (\rho_p - \rho)$ and g is the local gravity acceleration. The third term is the added-mass force, calculated via the added-mass coefficient, C_A, whose value will be set in $C_A = 2$, in accordance with the results of Jan and Chen [1]. The fourth term is the rolling resistance, that is obtained from the summation of force moments, with respect to the center of mass, and assuming a non-slip condition between the sphere and the plane:

$$F_R = \frac{2}{5}\rho_p\frac{4}{3}\pi r^3\frac{dU}{dt}. \quad (3)$$

If this last equation is substituted in Eq. (2), after rearrange terms, the following differential equation for $U(t)$ is obtained:

$$\frac{4}{3}\frac{\Delta\rho}{\rho}gdSin(\theta) - C_D U^2 = \frac{4}{3}d\left(\frac{7}{5}\frac{\rho_p}{\rho} + C_A\right)\frac{dU}{dt}. \quad (4)$$

Now, if the Eq. (1) is introduced into Eq. (4) with $Re = Ud/\nu$, it follows that:

$$a - AU^2 - \frac{B\nu}{Ud}U^2 = b\frac{dU}{dt} \quad (5)$$

where $a = 4/3\Delta\rho/\rho gdSin(\theta)$ and $b = 4/3d(7/5\rho_p/\rho + C_A)$.

It must be noted that Eq. (1), obtained for the steady regime of motion of the sphere, is assumed valid to model the motion in the transient regime. This assumption, that was used in previous works [3,5], can be supported by the fact that the particles, rolling down in slightly inclined planes, reach accelerations whose values are significantly lower than the value of the component of the gravity along the plane (see Fig. 12 in [3]). On the other hand, the relevance of this hypothesis can be inferred by the good agreement between theoretical and experimental results presented in the next section.

Rearranging terms, an ordinary differential equation for $U(t)$ is obtained:

$$m_0 - m_1 U - m_2 U^2 = \frac{dU}{dt} \quad (6)$$

where $m_0 = a/b$, $m_1 = B\nu/(bd)$, and $m_2 = A/b$.

This last equation is analogous to that found in previous studies [3]. Unlike the previously discussed works, a direct integration of this differential equation is proposed, by means of primitive functions.

If $U_0 < U(t)$, a first integration with respect to time, t can be performed:

$$-m_2 t = \int_{U_0}^{U}\frac{dU}{(U-\alpha_1)(U-\alpha_2)} \quad (7)$$

where the roots of the factorization for the second-order polynomial are:

$$\alpha_1 = \frac{m_1}{2m_2}\left[\left(1+\frac{4m_0m_2}{m_1^2}\right)^{1/2}-1\right] = \frac{m_1}{2m_2}(D-1) \tag{8}$$

and

$$\alpha_2 = -\frac{m_1}{2m_2}\left[\left(1+\frac{4m_0m_2}{m_1^2}\right)^{1/2}+1\right] = -\frac{m_1}{2m_2}(D+1) \tag{9}$$

where

$$D = \left(4m_0m_2/m_1^2+1\right)^{1/2}. \tag{10}$$

The integral in the right hand side of Eq. (7) can be explicitly solved, as shown in the Appendix A, giving as a result the velocity of the center of mass of the sphere, U, as a function of time, t:

$$U(t) = \frac{\alpha_2 e^{-m_1Dt}-\alpha_1\epsilon}{e^{-m_1Dt}-\epsilon} \tag{11}$$

where ϵ is defined as:

$$\epsilon = \frac{U_0-\alpha_2}{U_0-\alpha_1}. \tag{12}$$

The terminal velocity, U_t, can be obtained from Eq. (6) by making $dU/dt = 0$. Equivalently, the same result can be obtained by taking the limit $t \to \infty$ in Eq. (11):

$$U_t = \alpha_1. \tag{13}$$

The so-called terminal time, T, is defined as the time required by the velocity of the sphere to reach to 99% of U_t [2]. Since $U_0 < U_t$, ϵ is negative and, therefore, an analytical expression for T can be obtained:

$$T = \frac{1}{m_1D}ln\left(\frac{C}{|\epsilon|}\right) \tag{14}$$

where C is defined as:

$$C = \frac{\frac{D+1}{D-1}+0.99}{1-0.99} \approx \frac{200}{D-1}. \tag{15}$$

In the expression above, $C > 0$ because $D > 1$.

The coordinate of the center of mass of the sphere along the inclined plane, X, as a function of time, t, is obtained solving the following integral:

$$X(t) = X_0 + \int_0^t \frac{\alpha_2 e^{m_2\alpha t}dt}{e^{m_2\alpha t}-\epsilon} - \int_0^t \frac{\alpha_1\epsilon dt}{e^{m_2\alpha t}-\epsilon}. \tag{16}$$

Both integral terms in the right hand side are solvable, via substitution techniques, in terms of closed analytical functions, see the Appendix B. The final expression for $X(t)$ is:

$$X(t) = X_0 + \alpha_1 t + \frac{1}{m_2}ln\left(\frac{e^{-m_1Dt}-\epsilon}{1-\epsilon}\right). \tag{17}$$

The distance, L_t, that the sphere travels along the plane until reaching U_t, can be calculated by replacing $t = T$ in Eq. (17):

$$L_t = \frac{\alpha_1}{m_1D}ln\left(\frac{C}{|\epsilon|}\right) + \frac{1}{m_2}ln\left(\frac{1+1/C}{1+1/|\epsilon|}\right). \tag{18}$$

The next section presents and discusses experimental results, that show the influence of the size and density of the sphere, as well as the slope angle, on the transient phase of the longitudinal motion of the sphere. The predictive power of Eq. (17) is also discussed and analyzed.

3. Experimental results

Experiments were performed in a glass-walled tank, 50 cm long and 25 cm wide, filled with water, 24 cm depth, as shown schematically in Fig. 2. The water temperature was registered for each case, and their values were of around 16.5 °C. For this temperature the density and kinematic viscosity of water are $\nu = 0.011$ cm^2/s and $\rho = 0.999$ g/cm^3, respectively.

A glass plate, 50 cm long and 24 cm wide, was placed submerged in the tank. The edge of the plate closer to the position where the spheres were released (starting from rest) was kept submerged at a constant depth of 20, 5 cm. Two values of the slope, θ, were used: 6.5° and 15.4°. This was achieved varying the height of the support of the other edge of the plate (see Fig. 2).

Spheres of glass and steel, with three diameters, 6 mm, 4 mm and 2 mm, were used. Thus, the ratio between the sphere diameter and the tank width is small, and, based on the results of Jan and Chen [1], the influence of lateral confinement on the values of C_D can be neglected. The density of the spheres was calculated from the quotient M_T/V_T, where M_T and V_T are respectively, the mass (measured in a precision scale) and the volume (calculated from measurements of the diameters with a precision caliper) of a batch of similar spheres.

The spheres were released from rest ($U_0 = 0$) at a starting point located 10 cm from the top edge of the glass plate. An acrylic vertical tube was used to hold by hand a sphere (that is enclosed by the inner tube wall) at the starting point. The tube, in contact with the glass plate, is gently lifted upward a few sphere diameters, to minimize perturbations on the surrounding fluid, and then the sphere is free to roll downward in contact with the glass plate.

The motion of the sphere was recorded with a monochrome CCD camera JAI Pulnix DualTap Accupixel (640 × 480 pixels), at 100 frames per second. The physical scale (pixels to centimeters) was obtained from snapshots of a ruler placed over the submerged glass plate. The movies were processed with an ImageJ macro (www.nih.gov/ImageJ). As a result, the coordinates of the center of mass of the sphere, (X, Y), are obtained for each movie frame.

Fig. 3 presents typical results for the time evolution of X and Y in two different configurations. In both cases, the sphere diameter and the slope were held constant, $d = 0.394$ cm and $\theta = 6.5°$, respectively, and the densities of the spheres were different: (A) steel, $\rho_p = 8.1$ g/cm^3, and (B) glass, $\rho_p = 2.6$ g/cm^3. On each graph the left vertical

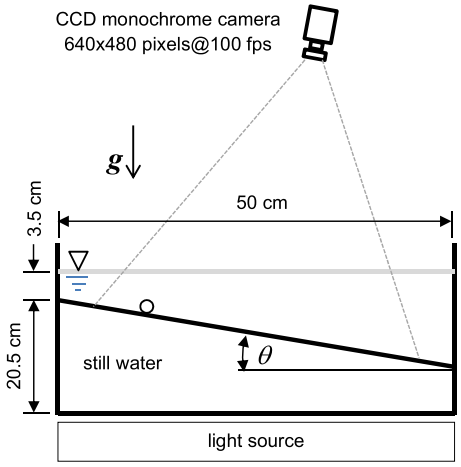

Fig. 2. Experimental setup (not drawn to scale).

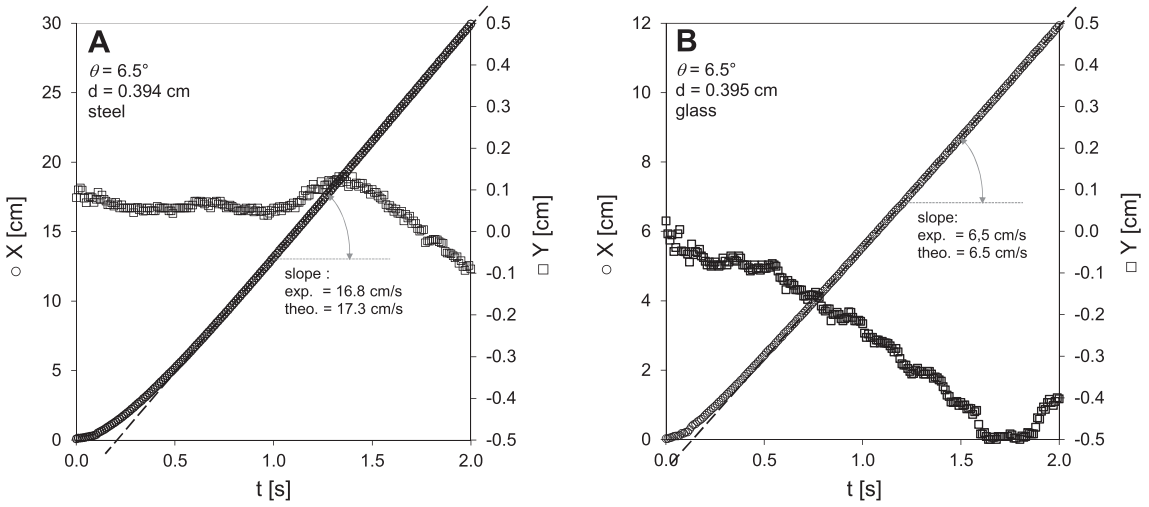

Fig. 3. Time evolution of the center of mass coordinates X and Y for a sphere, $d = 0.394$ cm, rolling down an inclined plane of slope $\theta = 6.5°$, for two different materials: (A) steel, $\rho_p = 8.1$ g/cm^3, and (B) glass, $\rho_p = 2.6$ g/cm^3. Markers are: ○ longitudinal coordinate along the plane, X, and □ lateral coordinate, Y.

axis corresponds to X (circular markers), and the right vertical axis corresponds to Y (square markers).

It is observed that transversal deviations from the central axis (given by Y) are generally small, remaining always within one sphere diameter. Furthermore, deviations are slightly larger for the glass spheres than for the steel ones. The glass spheres have a tendency to move in more sinuous paths when compared to steel ones. This behavior is probably due to imperfections on the glass surface of the sphere, that are not present in the steel ones. Another source of lateral deviations is the lower weight of the glass spheres, resulting in an a lower driving force for this particles, with respect to the steel ones, which implies an increased sensitivity to the presence of impurities or dust on the plate surface. Nevertheless, the size of the deviations, measured as the ratio between the maximal lateral deviation and the length of the total path is less than 10^{-2}. This result supports the hypothesis that spheres roll down following almost straight paths.

Measurements in Fig. 3 also show that the longitudinal coordinate along the plane, X, grows monotonically with time, t. Note that, in the same time interval, the sphere made of steel travels a distance that is 2.5 times larger than the distance traveled by the glass sphere. A dashed gray line is drawn along the linear portion of the curves of X against t, in order to put in evidence that there exists a finite time interval where the curves depart from this linear trend. Thus, two regimes of motion can be identified: an initial short phase, where the motion is strongly accelerated, that corresponds with the non-linear portion of the curves of $X(t)$, followed by a long-term phase, where a trend practically linear, associated with the motion at constant terminal velocity is observed. Related to this last point, the experimental and theoretical values of terminal velocity have been included in the plots under discussion. The first one is obtained as the slope of the curves of $X(t)$ in the linear regime, and the theoretic, by using Eq. (13). As can be observed, the values are in good agreement in both cases.

Regarding this last regime of motion at terminal velocity, Fig. 4(A) shows a direct comparison, between values of U_t from the works previously cited, in abscissa, and those predicted by Eq. (13), in ordinates. The same comparison is presented for T, Eqs. (14), and L_t, Eq. (18), and in Fig. 4(B) and (C), respectively. The three plots show that predictions of Eqs. (13), (14), and (18) are in good agreement with results of previous works, for a wide range of terminal velocities.

The influence of the slope, θ, on the temporal evolution of X, is shown in Fig. 5. In this case, a glass sphere, $\rho_p = 2.6$ g/cm^3, of diameter $d = 0.593$ cm, falls down along the inclined plane for two slope angles: □ 15.4°, and ○ 6.5°. The curves predicted by the analytical solution, Eq. (17), are also included for direct comparison. In the same graph, in vertical and horizontal dashed gray lines, the terminal time T, Eq. (14), and the traveled length $X(T) = L_t$, Eq. (18), respectively are also displayed. As expected, for given values of sphere density and diameter, the higher the slope, the faster is the motion of the sphere down along the inclined plane. As it can be observed, the curves predicted by Eq. (17) (in dashed black lines), are in good agreement with the experimental results in both cases.

Let's consider now the influence of the sphere density. Fig. 6 presents experimental results of X vs. t, for the same diameter of the spheres, $d = 0.395$ cm, and the same slope of the inclined plane, $\theta = 15.4°$, but with

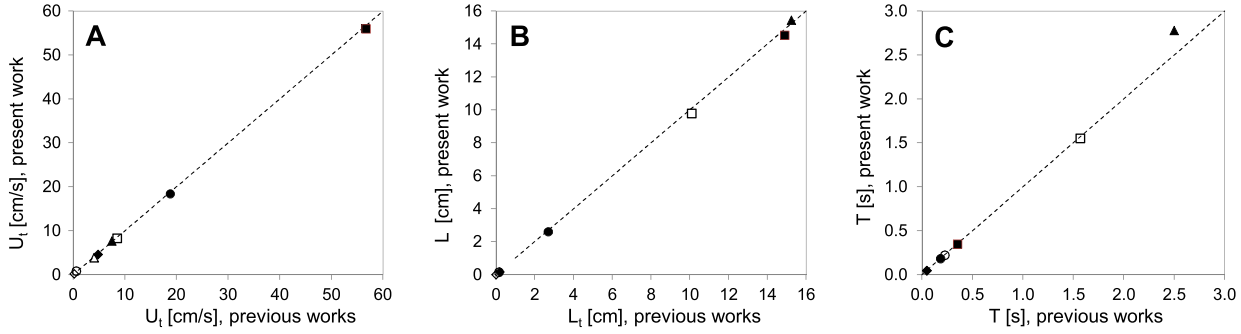

Fig. 4. Comparison between values of U_t, T, and L_t from previous works, and predictions of Eqs. (13), (14), and (18). In the three plots, markers are: ○ [2] water-glycerin solution 75% $\theta = 2°$, steel, $d_p = 3.96$ mm, • [2] water-glycerin solution 75% $\theta = 60°$, steel, $d_p = 3.96$ mm, □ [2] water $\theta = 2°$, steel, $d_p = 3.96$ mm, ■ [2] water $\theta = 60°$, steel, $d_p = 3.96$ mm, ◇ [2] oil $\theta = 2°$, steel, $d_p = 3.96$ mm, ◆ [2] oil $\theta = 2°$, steel, $d_p = 3.96$ mm, △ [5] water $\theta = 1.8°$, acrylic, $d_p = 25.8$ mm and ▲ [5] water $\theta = 5.7°$, acrylic, $d_p = 25.8$ mm.

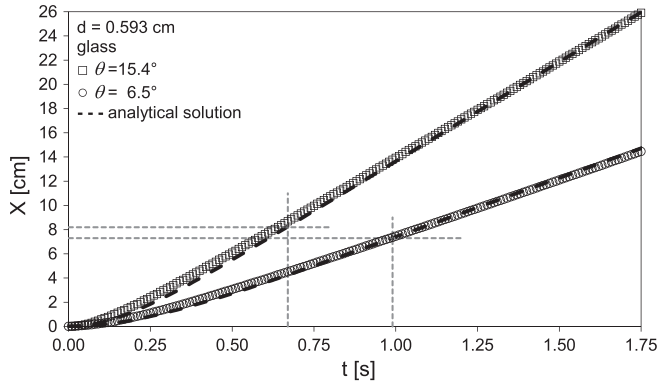

Fig. 5. Time evolution of the longitudinal coordinate for the center of mass along the inclined plane, X, for rolling spheres of glass, $\rho_p = 2.6$ g/cm^3, diameter $d = 0.593$ cm, for two slope angles: □ 15.4°, and ○ 6.5°. Black dashed lines show the prediction from Eq. (17). Vertical and horizontal gray dashed lines show the predictions for T and L_t, Eqs. (14) and (18), respectively.

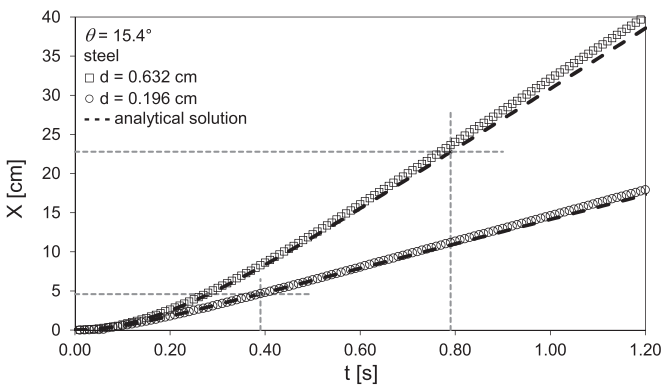

Fig. 7. Time evolution of the longitudinal coordinate for the center of mass along the inclined plane, X, for spheres of steel with the same slope $\theta = 15.4°$ and different sizes: □ $d = 0.632$ cm with $\rho_p = 7.9$ g/cm^3, and ○ $d = 0.196$ cm with $\rho_p = 8.2$ g/cm^3. Black dashed lines show the prediction from Eq. (17). Vertical and horizontal gray dashed lines show the predictions for T and L_t, Eqs. (14) and (18), respectively.

two different densities: □ steel, $\rho_p = 8.1$ g/cm^3, and ○ glass, $\rho_p = 2.6$ g/cm^3.

As it can be observed, if the slope and the diameter are held constant, the higher the density of the particle, the faster is the motion of the sphere along the plane. It is also observed that the model prediction (in dashed black lines) fits the measured values with good agreement. The values of T, Eq. (14), and $X(T) = L_t$, Eq. (18), are also displayed as vertical and horizontal dashed gray lines, respectively. It is noteworthy that a significant increase in sphere density (approximately three times), produces only a slight increase in the terminal time, T, but a large increase in the traveled distance, $L_t = X(T)$.

The third variable, whose influence was explored, is the sphere diameter. Fig. 7 presents two graphs of X vs. t for the case of two spheres of steel, moving along an inclined plane with the same slope $\theta = 15.4°$, for two different diameters: □ $d = 0.632$ cm ($\rho_p = 7.9$ g/cm^3), and ○ $d = 0.196$ cm ($\rho_p = 8.2$ g/cm^3). As in the previous cases, the prediction of the analytical solution, Eq. (17), in dashed black lines, is in good agreement with experimental results. It is also displayed, in both graphs, the predictions of Eqs. (14), for terminal time T, and (18), for $X(T) = L_t$, as vertical and horizontal dashed gray lines, respectively. In particular, note that in the same time interval, the small sphere travels less than a half of the distance traveled by the larger sphere.

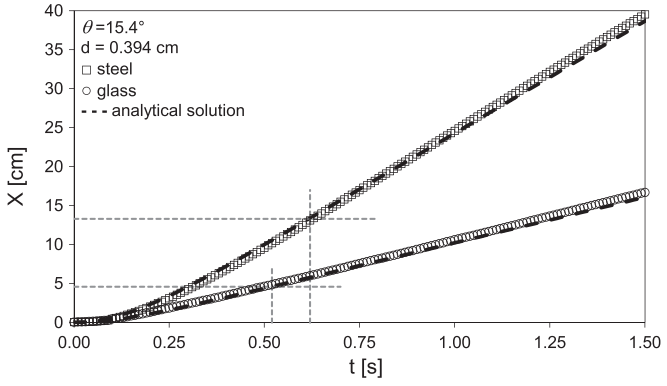

Fig. 6. Time evolution of the longitudinal coordinate for the center of mass along the inclined plane, X, for two rolling spheres of the same diameter $d = 0.395$ cm and slope $\theta = 15.4°$, for two different materials: □ steel, $\rho_p = 8.1$ g/cm^3, and ○ glass, $\rho_p = 2.6$ g/cm^3. Black dashed lines show the prediction from Eq. (17). Vertical and horizontal gray dashed lines show the predictions for T and L_t, Eqs. (14) and (18), respectively.

The velocity $U(t)$ can be calculated, from the raw measurements of X against t, via a numerical differentiation. It can be used a second order derivative in the form:

$$U = \frac{X(t+h) - X(t-h)}{2h} \tag{19}$$

where $h = 0.01$ s is the time interval between two consecutive frames of the recorded movies. It is interesting to follow the time evolution of U, in order to check that an asymptotic state of motion, with a constant terminal velocity, is really reached. This also allows the comparison between values of U from experimental data, and those predicted by Eq. (11).

Fig. 8 presents the measurements for the time evolution of X in continuous black line (left vertical axis), and U in open square markers (right vertical axis). The spheres have the same diameter, $d = 0.394$ cm, and roll down along the same slope, $\theta = 6.5°$, for two different materials: (A) steel, $\rho_p = 8.1$ g/cm^3, and (B) glass, $\rho_p = 2.6$ g/cm^3. In dashed black lines are shown the predictions of Eqs. (17) and (11), respectively.

As it can be observed, the spheres clearly reach a terminal velocity, with all points grouped around a horizontal plateau, whose values are in close agreement with those predicted by Eq. (13): $U_t = 17.3$ cm/s in Fig. 8(A), and $U_t = 6.5$ cm/s in Fig. 8(B). As it was previously observed, if the diameter and the density are held constant, the larger the slope the larger the terminal velocity and the distance needed to reach this terminal velocity. Note that, in the same time span, the steel sphere travels a distance that is twice the distance traveled by the glass sphere.

With respect to the model performance, it is concluded that time evolution of U is properly captured by Eq. (11). Similar trends of experimental results and model performance were observed in the cases previously analyzed in this section.

Finally, with the aid of the Eq. (17), a short discussion about the role of the added-mass and the rolling of the sphere it is offered, since both, the force of added-mass and the friction resistance, are proportional to the diameter, d, multiplied by the time derivative of velocity, $dU(t)/dt$. This is shown explicitly in the right hand side of Eq. (4), through the term:

$$\frac{4}{3} d \left(\frac{7}{5} \frac{\rho_p}{\rho} + C_A \right). \tag{20}$$

Thus, these terms only influence in the early stages of the motion of the sphere, since $dU(t)/dt$ vanishes when the sphere reaches terminal velocity, where the motion is governed by the balance between drag

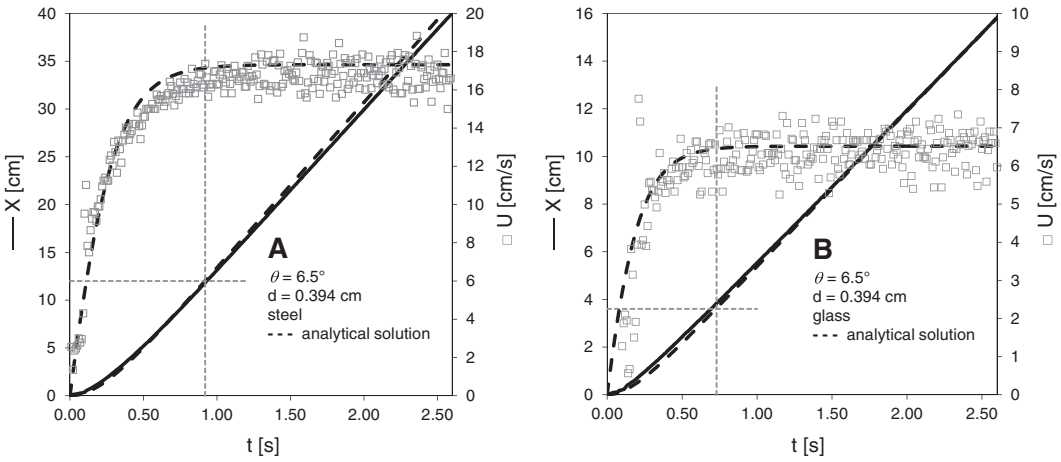

Fig. 8. Time evolution of (−) X and (□) U, for a sphere of diameter $d = 0.394$ cm and slope angle $\theta = 6.5°$, for two materials: (A) steel, $\rho_p = 8.1$ g/cm^3, and (B) glass, $\rho_p = 2.6$ g/cm^3. Black dashed lines show the prediction from Eqs. (17) and (11), respectively. Predictions from Eqs. (14) and (18) are shown in vertical and horizontal dashed gray lines. Terminal velocities from Eq. (13) are: (A) $U_t = 17.3$ cm/s, and (B) $U_t = 6.5$ cm/s.

force and submerged weight. In addition, heavier spheres (as a combination of a large diameter with high density) will be more affected by these terms, being higher, in these cases, the time span during which these spheres are under accelerated motion. By contrast, lighter spheres (small diameter and low density) will have a behavior as almost a point-like mass, reaching faster the asymptotic regime.

Based on the analytical equations previously discussed, the influence of these two forces can be explored if the corresponding terms are "turned off" in Eq. (17). This can be achieved making $C_A = 0$ and by replacing the factor 7/5 for 1 (this implies to neglect the rolling motion of the sphere). This is equivalent to consider a point-like mass that slides under gravity, along an inclined plane, without dynamic friction.

Fig. 9 illustrates the results obtained for different combinations of both, diameters and densities, maintaining constant the slope $\theta = 6.5$ *deg*. The rigid body model, Eq. (17), is shown in dashed black lines, whereas the frictionless point-like mass model is shown in dotted black lines. As expected, for the three cases it is observed that, if the rolling of the particle and the force of added-mass are discarded, the distances traveled by the sphere are larger. The difference between models is larger for the case of the heavier particle, see plot (A), and very small in the case of the lighter particle, see plot (C). At the same time, the terminal velocity (the slope of $X(t)$ in the linear portion of the curve), does not change from one model to the other, since U_t arises from the balance of constant forces (drag and submerged weight) at the asymptotic regime of motion.

Nevertheless, and more important, it must be emphasized that a point-like mass, sliding along a frictionless inclined plane, is not a realistic approach to the problem under discussion, since the dynamic friction cannot be discarded from the analysis. Furthermore, the simplified model performance gets worse as the value of the diameter and/or the density of the sphere increases, which, in turn, highlights the relevance of the full model.

4. Conclusions

We have reported an experimental study of the transient motion of a sphere, moving downhill along an inclined plane submerged in quiescent water. Several experiments were performed in a water tank, varying systematically the diameter and density of the spheres, as well as the slope angle of the inclined plane.

The spheres were released from rest, and its motion was recorded with high temporal resolution. This allowed properly capturing of the accelerated (transient) phase of motion of the spheres, before they reach motion at constant velocity.

The measurements show that the sphere moves following almost straight paths. The temporal evolution of the longitudinal coordinate,

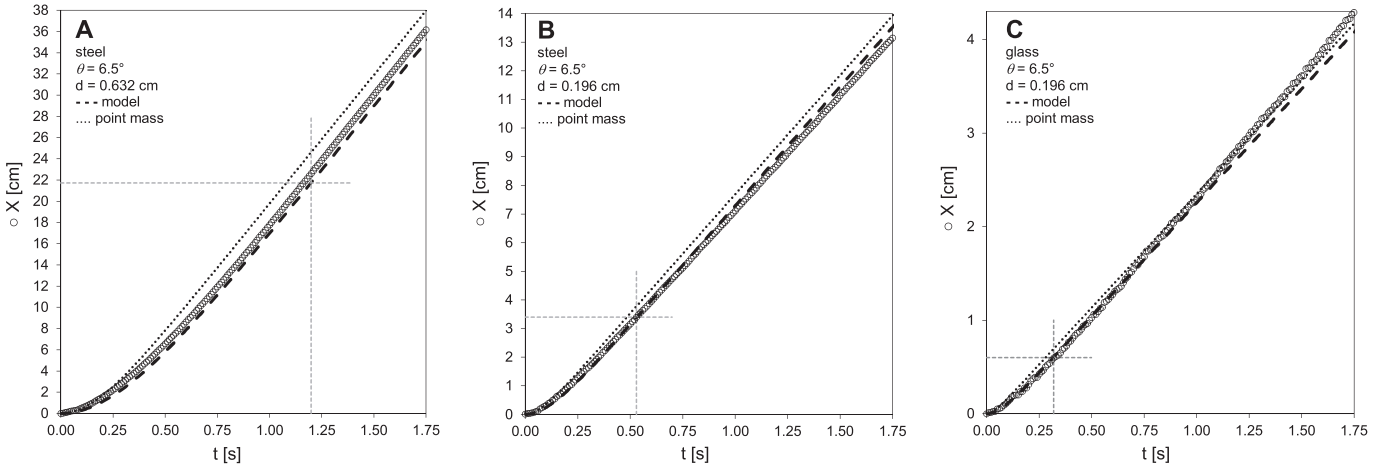

Fig. 9. Time evolution of (○) X for rolling spheres along a plane of slope $\theta = 6.5°$, for: (A) steel, $d = 0.632$ cm, (B) steel, $d = 0.196$ cm, and (C) glass, $d = 0.196$ cm. Black dashed lines correspond to the model prediction, Eq. (17). Dotted black lines correspond to the prediction of a model for a point mass that descends on an inclined plane with negligible friction.

X, reveals two regimes of motion: a first short-time interval, where X shows a nonlinear trend with t, that corresponds with an accelerated motion, followed by a regime of motion where a linear trend is observed, associated to a second phase of motion at constant velocity, the so-called terminal velocity.

An analytical equation for the longitudinal motion of the center of mass of the sphere, X, as function of the time, t, is obtained by direct integration of the dynamical equations of motion, by assuming that the sphere behaves as a rigid body that rolls down, along a smooth inclined plane, without sliding. As a part of the integration process, we have also obtained an explicit equation for $U(t)$, the longitudinal component of the velocity of the center of mass of the sphere. The forces acting over the sphere are: drag, lift, weight, buoyancy, rolling resistance, normal reaction, and the force of added-mass. In the formulation of the drag force of the fluid over the sphere we used the correlation proposed by Chhabra and Ferreira [2], for the experimental results of Jan and Chen [1], between the drag coefficient, C_D, and the Reynolds number of the sphere.

A good agreement between the experimental results and the predictions from the explicit expression of $X(t)$, in a wide range of experimental conditions is observed.

Explicit equations are also presented for U_t, L_t, and T as functions of θ, d, and ρ_p, as well as of fluid density and viscosity. Predictions from these equations show good agreement with results of previous works, also in a wide range of configurations.

Some interesting perspectives emerge when considering other more complex cases, which would enable to test the validity of the model. For example, the motion of a sphere along a rough and/or slightly wavy plane, or in high slope conditions, where the hypothesis of rolling without sliding presumably is no longer valid. Because of the practical importance of developing models to accurately predict the dynamics of particles, some of these issues must be addressed in future work.

Acknowledgment

The authors gratefully acknowledge the financial support from Universidad de Buenos Aires (UBACyT 20020100100853).

Appendix A. Integration for $U(t)$

The right hand side of Eq. (7) can be rewritten in the following way:

$$\int_{U_0}^{U}\frac{dU}{(U-\alpha_1)(U-\alpha_2)}=\int_{U_0}^{U}\left(-\frac{dU}{\alpha(U-\alpha_1)}+\frac{dU}{\alpha(U-\alpha_2)}\right) \tag{A.1}$$

where $\alpha=\alpha_2-\alpha_1$. This term can be directly integrated:

$$\int_{U_0}^{U}\frac{dU}{(U-\alpha_1)(U-\alpha_2)}=\frac{1}{\alpha}\left[-ln\left(\frac{U-\alpha_1}{U_0-\alpha_1}\right)+ln\left(\frac{U-\alpha_2}{U_0-\alpha_2}\right)\right] \tag{A.2}$$

where $ln()$ is natural logarithm. The above expression can be rewritten as:

$$\int_{U_0}^{U}\frac{dU}{(U-\alpha_1)(U-\alpha_2)}=\frac{1}{\alpha}ln\left(\frac{\frac{U-\alpha_2}{U_0-\alpha_2}}{\frac{U-\alpha_1}{U_0-\alpha_1}}\right)=-m_2t \tag{A.3}$$

and, by taking exponential in both sides, leads to:

$$\frac{(U-\alpha_2)(U_0-\alpha_1)}{(U-\alpha_1)(U_0-\alpha_2)}=e^{-m_2\alpha t} \tag{A.4}$$

and, finally, after rearranging terms, it is obtained Eq. (11):

$$U(t)=\frac{\alpha_2e^{-m_1Dt}-\alpha_1\epsilon}{e^{-m_1Dt}-\epsilon} \tag{A.5}$$

where it was used the following:

$$m_2\alpha=m_2(\alpha_2-\alpha_1)=-m_1D \tag{A.6}$$

and ϵ is defined as:

$$\epsilon=\frac{U_0-\alpha_2}{U_0-\alpha_1} \tag{A.7}$$

Appendix B. Integration for $X(t)$

The first integral in the right hand side of Eq. (16) can be solved with the substitution $z=e^{m_2\alpha t}-\epsilon$. In doing this it is obtained:

$$\int_0^t\frac{\alpha_2e^{m_2\alpha t}dt}{e^{m_2\alpha t}-\epsilon}=\frac{\alpha_2}{m_2\alpha}ln\left(\frac{e^{m_2\alpha t}-\epsilon}{1-\epsilon}\right). \tag{B.1}$$

To solve the second integral in Eq. (16), it is proposed the substitution $z=e^{m_2\alpha t}$, that, when is replaced, leads to the following intermediate integrals:

$$\int_0^t\frac{\alpha_1\epsilon dt}{e^{m_2\alpha t}-\epsilon}=\frac{\alpha_1\epsilon}{m_2\alpha}\int_{z_0}^{z}\frac{dz}{z(z-\epsilon)} \tag{B.2}$$

that can be expanded via simple partial fractions in the following sum of terms:

$$\int_0^t\frac{\alpha_1\epsilon dt}{e^{m_2\alpha t}-\epsilon}=\frac{\alpha_1\epsilon}{m_2\alpha}\left(\int_{z_0}^{z}-\frac{dz}{\epsilon z}+\int_{z_0}^{z}\frac{dz}{\epsilon(z-\epsilon)}\right). \tag{B.3}$$

Finally, by direct integration it is obtained:

$$\int_0^t\frac{\alpha_1\epsilon dt}{e^{m_2\alpha t}-\epsilon}=\frac{\alpha_1}{m_2\alpha}\left[-ln\left(\frac{e^{m_2\alpha t}}{1}\right)+ln\left(\frac{e^{m_2\alpha t}-\epsilon}{1-\epsilon}\right)\right] \tag{B.4}$$

or, equivalently

$$\int_0^t\frac{\alpha_1\epsilon dt}{e^{m_2\alpha t}-\epsilon}=\frac{\alpha_1}{m_2\alpha}\left[-m_2\alpha t+ln\left(\frac{e^{m_2\alpha t}-\epsilon}{1-\epsilon}\right)\right]. \tag{B.5}$$

The substitution of the above terms in Eq. (16) leads to:

$$X(t)=X_0+\frac{\alpha_2}{m_2\alpha}ln\left(\frac{e^{m_2\alpha t}-\epsilon}{1-\epsilon}\right)-\left[\frac{\alpha_1}{m_2\alpha}ln\left(\frac{e^{m_2\alpha t}-\epsilon}{1-\epsilon}\right)-\alpha_1t\right] \tag{B.6}$$

$$X(t)=X_0+\alpha_1t+\frac{(\alpha_2-\alpha_1)}{m_2\alpha}ln\left(\frac{e^{m_2\alpha t}-\epsilon}{1-\epsilon}\right) \tag{B.7}$$

and, again, by virtue of the equalities $\alpha=\alpha_2-\alpha_1$ and $m_2\alpha=-m_1D$, the following final expression is obtained:

$$X(t)=X_0+\alpha_1t+\frac{1}{m_2}ln\left(\frac{e^{-m_1Dt}-\epsilon}{1-\epsilon}\right). \tag{B.8}$$

References

[1] C. Jan, J. Chen, Movements of a sphere rolling down an inclined plane, J. Hydraul. Res. 35 (5) (1997) 689–706.
[2] R.P. Chhabra, J.M. Ferreira, An analytical study of the motion of a sphere rolling down a smooth inclined plane in an incompressible Newtonian fluid, Powder Technol. 104 (2) (1999) 130–138.
[3] M. Jalaal, D.D. Ganji, An analytical study on motion of a sphere rolling down an inclined plane submerged in a Newtonian fluid, Powder Technol. 198 (1) (2010) 82–92.
[4] R. Ebrahimi Naghani, S.D. Farahani, M.R. Davoudabadi, Application of differential transformation method to study on motion of a sphere rolling down an inclined plane submerged in incompressible Newtonian media, World Appl. Sci. J. 11 (9) (2010) 1138–1147.
[5] P. Verekar, J. Arakeri, Sphere rolling down an incline submerged in a liquid, Proceedings of 37th National and 4th International Conference on Fluid Mechanics and Fluid Power (FMFP10), India, 2010.